

Onset of Quantum-Confined Stark Effects in Multijunction Photovoltaic Laser Power Converters Designed with Thin Subcells

Simon Fafard * and Denis Masson

Broadcom (Canada), IFPD, Ottawa, ON K1A 0R6, Canada; denis.masson@broadcom.com

* Correspondence: simon.fafard@broadcom.com

Abstract: Photovoltaic multijunction power-converting III–V semiconductor devices generate electrical power from the optical energy of laser beams. They exhibit conversion efficiencies reaching values greater than 60% and 50% for the GaAs and the InP material systems, respectively. The applications of optical wireless power transmission and power-over-fiber greatly benefit from employing such laser power converters constructed with multiple subcells; each is designed with either thin GaAs or InGaAs absorber regions. This study elucidates how the application of electric fields on thin heterostructures can create specific current–voltage characteristics due to modifications of the absorption characteristics from Franz–Keldysh perturbations and the onset of quantum-confined Stark effects. Negative differential photocurrent behavior can be observed as the reverse bias voltage is increased, until the corresponding current-clamping subcell reaches its reverse breakdown condition. The reverse voltage breakdown characteristics of the subcells were also measured to depend on the thickness of the subcell and on the optical intensity. The onset of the reverse breakdown was found to be at ~2.0–2.5 V under illumination and the thinner subcells exhibited higher levels of reverse bias currents. These effects can produce distinctive current–voltage behavior under spectrally detuned operations affecting the thinner subcells’ biases, but have no significant impact on the performance and maximum power point of multijunction power converters.

Keywords: optical power converters; laser power converters; power-over-fiber; power beaming; photovoltaic; Franz–Keldysh effect; quantum-confined Stark effect; galvanic isolation; GaAs; InGaAs; AlGaAs; InGaP; InP; multijunction semiconductor heterostructures; photonic power converters

**Citation:** Fafard, S.; Masson, D.Onset of Quantum-Confined Stark Effects in Multijunction Photovoltaic Laser Power Converters Designed with Thin Subcells. *Photonics* **2023**, *10*, 1243. <https://doi.org/10.3390/photronics10111243>

Received: 27 September 2023

Revised: 2 November 2023

Accepted: 6 November 2023

Published: 8 November 2023



Copyright: © 2023 by the authors. Licensee MDPI, Basel, Switzerland. This article is an open access article distributed under the terms and conditions of the Creative Commons Attribution (CC BY) license (<https://creativecommons.org/licenses/by/4.0/>).

1. Introduction

It is well established that the optical properties of semiconductor materials are affected by electric fields. In bulk III–V materials, the Franz–Keldysh effect generates a tail in the absorption coefficient below the absorber’s bandgap, as well as spectral oscillations of the absorption coefficient for energies above the absorber’s bandgap value. Similarly, in low-dimensionality semiconductor structures, the corresponding quantum-confined Stark effect also modifies the material’s absorption coefficient. These effects have been thoroughly studied and exploited [1–11], especially in GaAs and InP-based devices benefiting from electric-field controlled electro-absorption properties in quantum wells made of GaAs or InGaAs absorbers. Concurrently, p/n photovoltaic (PV) devices have been optimized to convert laser power at different wavelengths [12–91]. Such devices are usually called Optical Power Converters (OPCs) or Laser Power Converters (LPCs) and have been shown to greatly benefit from heterostructure designs based on multiple subcells [12,48] instead of a thicker single p/n junction. This is because the voltage generated by an OPC or LPC increases with the number of series connected layers or subcells used in its design. For that reason, multijunction LPCs can be thought of as Photo-Transducers (PT for short), where the number of subcells determines the output voltage of the devices when subjected to illumination. Thus, a device built from a stack of a number, N , of light absorbing p/n junctions of the same type (e.g., all GaAs p/n junctions) is expected to generate an output

voltage approximately N times the voltage of one p/n junction. It is convenient then to refer to the active layers of OPCs and LPCs as PTN where PT refers to photo-transducer and N , the number of active absorbing p/n junctions used. Note that the highly doped p⁺⁺/n⁺⁺ tunnel junctions often used in OPCs and LPCs are usually designed with materials having a bandgap higher than the bandgap of the absorbing material (i.e., transparent to the incident optical beam). Therefore, the tunnel junctions do not contribute to the output voltage, except for a very small internal drop in voltage (typically only a few mV). The ability to design and fix the output voltage from the beginning is important for most practical applications where a specific voltage range is usually required and/or when the voltage and current must match the intended load impedance.

In the approach using series-connected subcells discussed above, a comparable fraction of the incident optical beam is absorbed in each subcell and the Beer–Lambert law is used as a good first approximation to design the individual thicknesses of the p/n junctions thus comprised of a stack of thinner subcells [22,23]. It should also be noted that for a given optical input wavelength, the total absorber thickness required to capture substantially all (e.g., 99%) the incident light is fixed. Therefore, PTN LPCs built with a larger N value are by design constructed with thinner subcells. Concurrently, PTN devices with different N values have similar total device thicknesses.

Compared to its constituent absorber material, such series-connected layers efficiently convert a high-power optical input, with a relatively narrow spectral range, into an electrical output. The output has an up-converted photovoltage and a correspondingly down-converted current in operation [42–44]. For a specified incident laser wavelength, a photocurrent-matching condition is realized by design, with the subcells having increasing thicknesses from the top subcell (thinnest) toward the bottom subcell (thickest). LPC devices with 12 subcells or more have been successfully realized. As the number of subcells is increased, the upper subcells need to be thinner than 100 nm [43–45]. The physics of these multijunction power converter devices is interesting with phenomena such as strong luminescence coupling and recycling [57–60], especially when the device is operated in de-tuned conditions, away from the peak of its spectral response. The study of spectrally de-tuned multijunction LPCs, designed with thin absorbing subcells, is therefore of particular interest to better understand the influence of applied electric fields on the properties of these devices. In addition, in typical p/n junctions, potential Franz–Keldysh effects occur in the depletion zone where the electric field is the strongest. Since the depletion zone is determined by doping levels rather than the overall thickness, the effects are expected to be more pronounced in thinner cells.

The present study demonstrates that the application of electric fields on heterostructures incorporating thin GaAs and InGaAs subcells can create distinctive current–voltage (I–V) characteristics. Negative differential photocurrent behavior can be observed as the bias voltage is swept from the photovoltaic (positive biases) to the photodiode (negative biases) mode of operation, until the corresponding current-clamping subcell reaches its reverse breakdown condition. Control single junctions (1Js) of different thicknesses are also studied and our overall results indicate that the observed negative differential photocurrent behavior of the multijunction device is due to modifications of the absorption characteristics from Franz–Keldysh or the onset of quantum-confined Stark effects. The results also confirm that these effects have no significant impact on the maximum power point of multijunction power converters while producing distinctive I–V behavior under spectral detuned operations.

2. Materials and Methods

The heterostructures are grown lattice-matched using commercial production Metal Organic Chemical Vapor Deposition (MOCVD) reactors from Aixtron. For the present study, the photovoltaic junction designs were all n/p, i.e., based on an n-type emitter nearest to the incident side of the light input. The LPCs with the GaAs absorbers are grown on GaAs substrates. They have AlGaAs and InGaP-based barriers and tunnel junctions between the

subcells' absorber regions [22]. For consistency, the thicknesses and doping levels of the tunnel junctions were kept substantially equivalent for the various multijunction designs with a different number of subcells. The longer-wavelength LPCs with the InGaAs absorbers are grown on InP substrates. They have InP and AlInGaAs-based barriers and tunnel junctions between the subcells' absorber regions [46]. Manufacturing microfabrication processes are used to transform the epitaxial wafers into chips. A chip area of $\sim 0.03 \text{ cm}^2$ is used here. The chips have corner pads and a contour busbar. The devices include standard blanket back-metallization, front ohmic contacts, and antireflection coatings (ARCs). The ARC is constructed from layers of Al_2O_3 and TiO_2 and typically reduces the reflectivity (R) of the incident beam to $R < 4\%$ for the spectral range of interest. From our overall experimentation, the details of the chip geometry are not particularly relevant to the specific phenomenon discussed in this study. The I–V characteristics were acquired with a Keithley 2601B source meter in the 4-wire probing mode. For the I–V measurements, the tip of a fiber-coupled laser was positioned in front of the device at near-normal incidence. The distance between the fiber tip and the PV device was adjusted to obtain the desired spot size from the diverging beam. Therefore, as is usually the case in typical operating conditions, non-uniform illumination is used in the experiments of this study [48]. The fiber laser had a numerical aperture of ~ 0.22 . The input lasers were operated in a continuous (CW) mode. Quick I–V scans were used to minimize any chip heating or temperature drifts between the measurements.

3. Results

Control 1Js of different thicknesses were also prepared using the processes described above. The related heterostructure details have been described in detail previously [22]. The thicknesses of the five control 1Js devices were between 212 nm and 2336 nm, as indicated in Figures 1 and 2. Figure 1 shows the measured dark I–Vs for all five 1Js, together with the 808 nm illuminated I–V characteristics for the thinnest control GaAs single junction: S5, having a thickness of 212 nm. Figure 2 shows the semi-log plot of the dark I–V curves of Figure 1 to better visualize the relative dark-current behavior of the 1Js designed with different thicknesses.

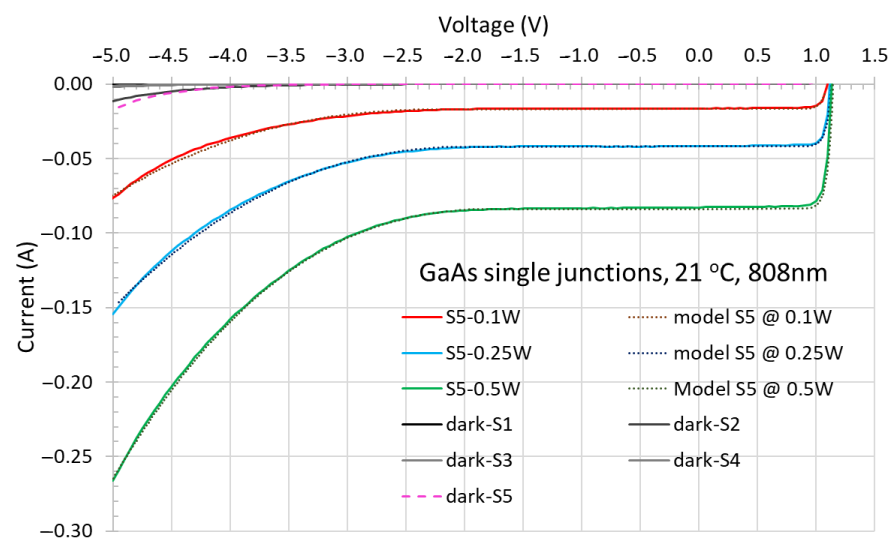


Figure 1. Measured I–V characteristics for thin control GaAs single junctions having different absorber thicknesses: dark-S1 is the dark I–V curve for a GaAs absorber 2336 nm thick, dark-S2 is for 581 nm, dark-S3 is for 346 nm, dark-S4 is for 246 nm, and dark-S5 is for 212 nm. Measured I–V curves are shown for S5 illuminated at 808 nm with optical input powers between 0.1 W and 0.5 W. The diode equation fit (model) to the illuminated I–V curves is shown with the dotted curves for each optical input power. The device area is 0.034 cm^2 . The dark-S1, dark-S2, dark-S3 and dark-S4 lines follow near the zero current horizontal axis, but are clearly revealed in Figure 2 using a logarithmic current axis.

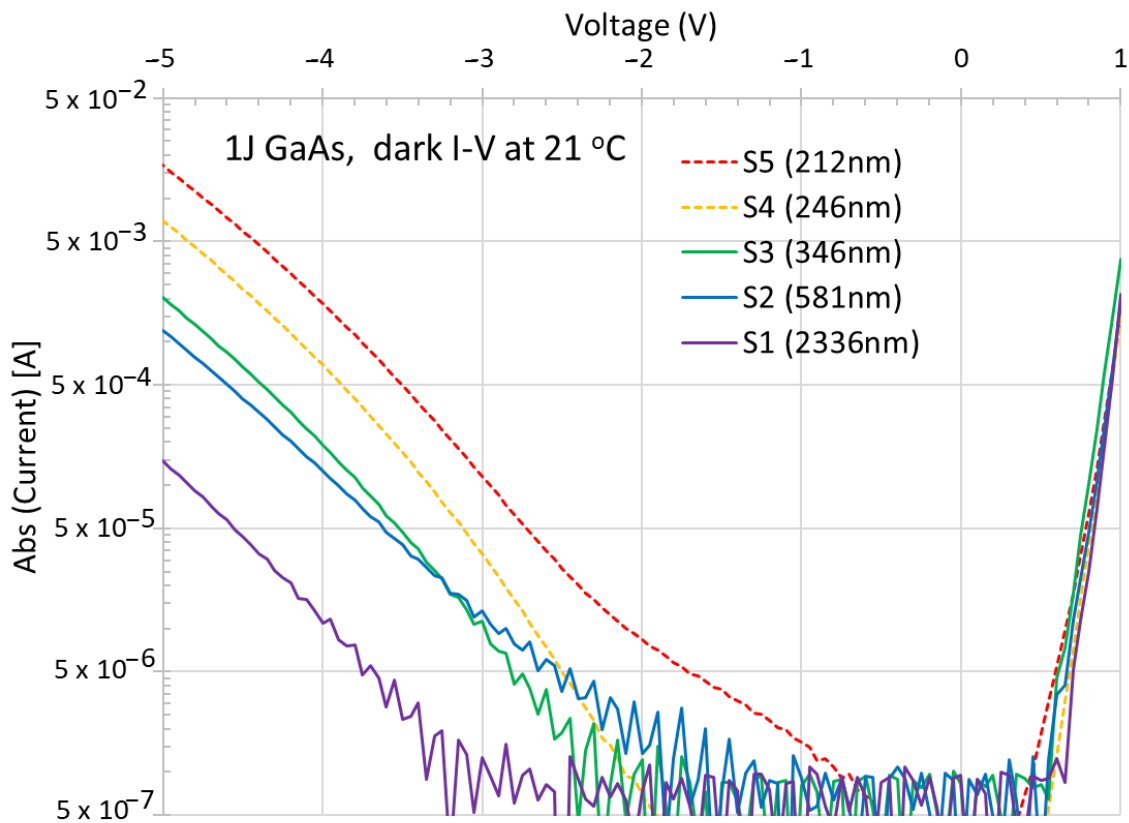


Figure 2. Semi-log plot of the dark I–V curves of Figure 1.

The illuminated I–Vs of Figure 1 are obtained with optical input powers between 0.1 W and 0.5 W. The diode equation fits (model) to the illuminated I–V curves are shown with the dotted curves. Good fits can be obtained using an ideal diode equation for the forward voltages $V > 0$. For simplicity, the reverse breakdown behavior is characterized by a power-law breakdown for $V < 0$:

$$\begin{aligned}
 I(V) &= -I_{sc} + I_0 [\exp(qV/nkT) - 1], V \geq 0 \\
 I(V) &= -I_{sc} - \alpha [V - V_{br}]^\beta, V < 0
 \end{aligned}
 \tag{1}$$

where I_{sc} is the zero-bias photocurrent or equivalently the short-circuit current, I_0 is the saturation current, n is the ideality factor, q is the charge of the electron, k is the Boltzmann’s constant, T is the temperature; and α , β , and V_{br} are empirical values used to characterize the breakdown current behavior. Ideality factors of $n = 1.6$ were used because values around 1.6 gave close to the best fits to the I–V curves, especially for the voltages between V_{mpp} and V_{oc} .

The onset of the reverse breakdown was in the range of negative ~ 2.0 to 2.5 V for the GaAs PV cells, depending on the illumination intensity. Moreover, the thinner subcells exhibit higher levels of reverse bias currents, as evidenced in Figure 2. Therefore, the reverse voltage breakdown characteristics of the subcells were measured to depend not only on the subcell thickness, but also strongly influenced by the incident optical intensity, as can be deduced from Figures 1 and 2.

It should also be noted that the subcell electrical field and the p/n depletion region width are expected to be influenced primarily by the doping levels and can also be affected by screening effects [7,8] from the photocarrier density. Precise quantitative modeling of these effects is beyond the scope of the present study. However, the control 1J device characteristics measured in Figures 1 and 2 can now be used to benchmark and better understand the behavior of multijunction LPCs.

Figure 3 compares the I–V characteristics of multijunction GaAs devices with a number of $N = 6, 8,$ and 10 subcells, hereby named PTN with N representing the number of subcells, as mentioned in the introduction. The peak of the spectral response of these LPCs was separately measured to be between 815 nm and 835 nm, with peak conversion efficiencies in excess of 60% [12,45,48].

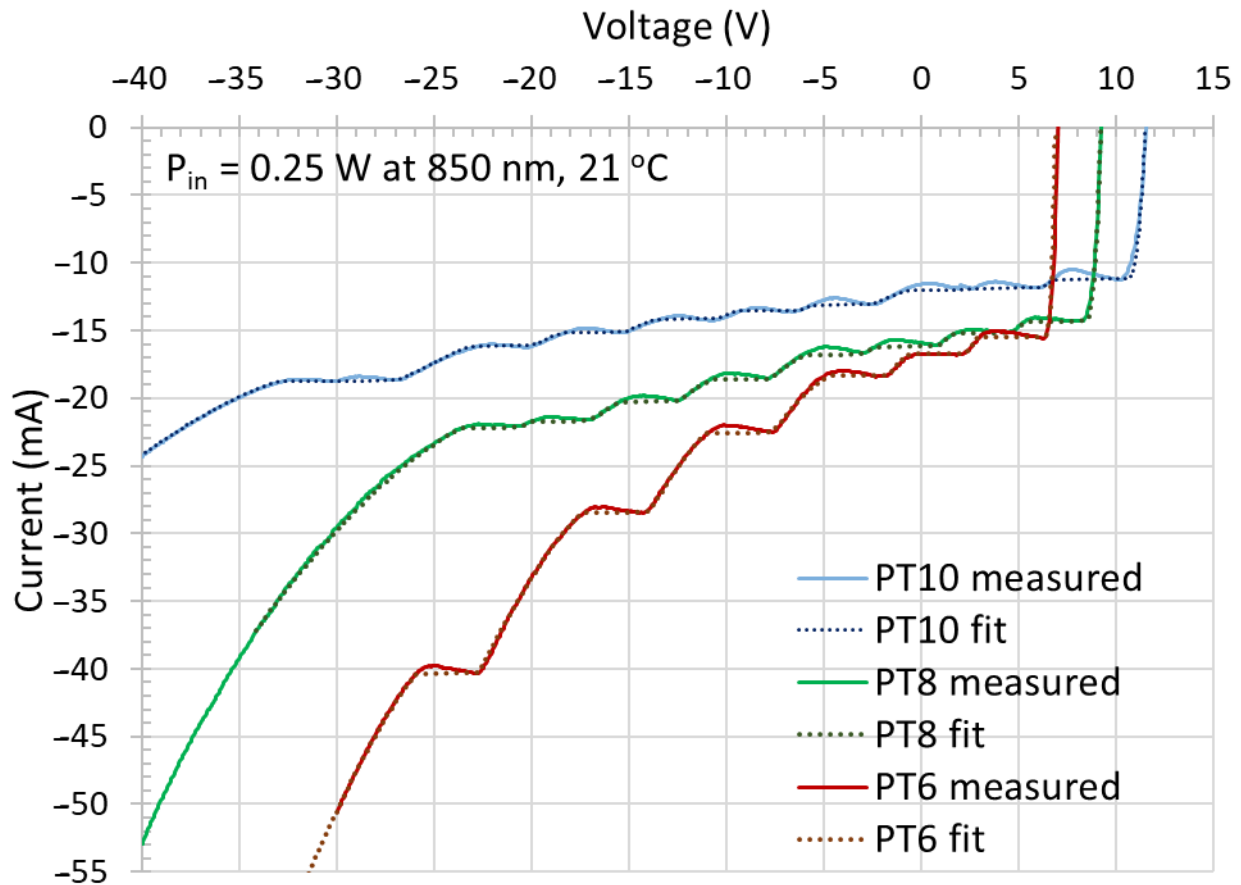


Figure 3. I–V characteristics of multijunction GaAs devices for 6, 8, and 10 subcells (named PTN with N representing the number of subcells). The I–V curves are measured with 0.25 W of optical input at 850 nm, detuned on the long wavelength side of the peak of the spectral response: i.e., current-limited by the upper subcells. The thicknesses of the thinnest upper subcells are: 127 nm, 120 nm, and 106 nm for PT6, PT8, and PT10 respectively. The diode equation fit to the illuminated I–V curves is shown with the dotted curves for each device. The area of the devices is 0.032 cm².

The optical input for Figure 3 was intentionally detuned by using a laser probe wavelength of 850 nm, with 0.25 W of optical input power. With the detuning being on the long wavelength side of the peak of the spectral response, the multijunction devices are therefore unambiguously current-limited by the upper subcell for a bias voltage around the maximum power point of their respective I–V curves: $V_{\text{mpp}} = 10.35$ V for the PT10, $V_{\text{mpp}} = 8.35$ V for the PT8, and $V_{\text{mpp}} = 6.40$ V for the PT6. As the applied voltage is swept in the reverse direction, away from V_{mpp} on the I–V curves, the current-clamping of the current-limiting subcell is maintained until the subcell reverse current breakdown is reached. Then, the next subcell becomes current-limiting and clamps the overall multijunction current. This cascade continues until all subcells are in reverse-breakdown mode. Consequently, the I–V curves of the multijunction devices feature the same number of current plateaus as the corresponding number of subcells. Indeed, 6, 8, and 10 plateaus are clearly observed in Figure 3 for PT6, PT8, and PT10, respectively. Similar plateaus have been reported previously. By biasing the multijunction device on a given plateau, the relative photocurrent of the corresponding subcell can be extracted at the probing wavelength. This method can be

useful for extracting the responsivity, the quantum efficiency, the absorption coefficients, and the spectral response information for the heterostructure [18,31,32,40,41,44].

Figure 3 also shows the diode equation fits to the illuminated I–V curves. The fits are shown with the overlapping dotted curves and incorporate N series-connected subcells based on Equation (1). As for the control 1Js, ideality factors of $n = 1.6$ were used for the fits. Moreover, the α , β , and V_{br} fitting values for the breakdown current behaviors used in Figure 3 are consistent with the behavior observed in Figure 1 for the control 1Js. For the PTN devices, the thicknesses of the thinnest upper subcells were further reduced to 127 nm, 120 nm, and 106 nm for the PT6, PT8, and PT10, respectively. By comparing the ideal diode fit to the measured I–V behaviors, it becomes apparent that slight photocurrent reductions are sometimes observed before the onset of the subcell’s reverse-bias breakdown. Such negative differential photocurrent behavior can be observed more clearly with the first plateau of the PT10 for the thinnest upper subcell (i.e., 106 nm). The photocurrent is reduced by ~6% as the reverse bias voltage is increased, until the corresponding current-clamping subcell reached its reverse breakdown condition. This is not expected from the ideal diode equation model. It justifies further analysis because, for the measured condition, such a photocurrent decrease suggests a reduction in the absorption coefficient under the applied electric field. The effect is further investigated in Figure 4 with PT12 having an even thinner upper subcell of 82 nm.

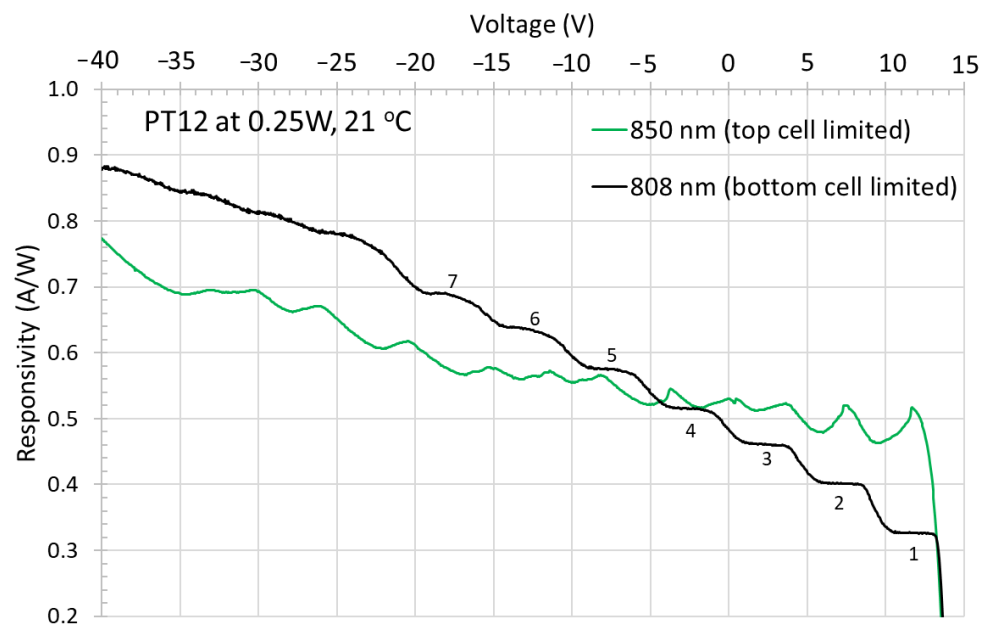


Figure 4. Measured I–V characteristics of a PT12 multijunction GaAs device with 12 subcells. The responsivity curves are measured with 0.25 W of optical input power, the device area is 0.032 cm² and the thickness of the thinnest upper subcell is 82 nm. The black curve is for a detuned condition on the short wavelength side of the peak of the spectral response: i.e., current-limited by the thicker bottom subcells. The green curve is for a detuned condition on the long wavelength side of the peak of the spectral response: i.e., current-limited by the thinner top subcells.

Figure 4 shows the measured I–V characteristics of a PT12 multijunction GaAs device with 12 subcells. The black curve shows the responsivity for a detuned condition on the short wavelength side of the peak of the spectral response. Under these conditions, the device is unambiguously current-limited by the thicker bottom subcells (here, 2211 nm thick). The observed plateaus are substantially flat, as expected for subcells with no significant changes to their absorption properties caused by applied electric fields. In drastic contrast, the green curve is for a detuned condition on the long wavelength side of the peak of the spectral response, and therefore current-limited by the thinner top subcells. For the 82 nm subcell (peak between 9 V and 12 V of the green curve), significant negative

differential photocurrent behavior can be observed as the reverse bias voltage is increased, until the corresponding current-clamping subcell reaches its reverse breakdown condition. It is worth pointing out that the effect was exemplified here with 12 subcells, but similar behavior has also been measured for devices with more subcells (e.g., PT20, not shown), or slightly lower number of subcells such as the PT10 of Figure 3.

4. Discussions

We observed that the negative differential photocurrent behavior is apparently enhanced for the thinner subcells (i.e., PTN with larger N). This is combined with the observation that these features are substantially absent for the conditions when the device is current-limited by the thicker bottom subcells (i.e., for a detuned condition on the short wavelength side of the peak of the spectral response). It strongly suggests that the thinner subcells support these particular I–V characteristics due to modifications of the absorption characteristics from Franz–Keldysh perturbations or the onset of quantum-confined Stark effects [4,11].

Similar behavior is also clearly observed for the other material system studied. These LPCs are using InGaAs as the absorbing subcells. They are for applications at wavelengths around 1.5 μm . For example, Figure 5 shows a semi-log plot of the measured I–V characteristics of a PT10 multijunction device with 10 InGaAs subcells lattice-matched to InP. For this heterostructure, the thickness of the thinnest upper subcell is 105 nm.

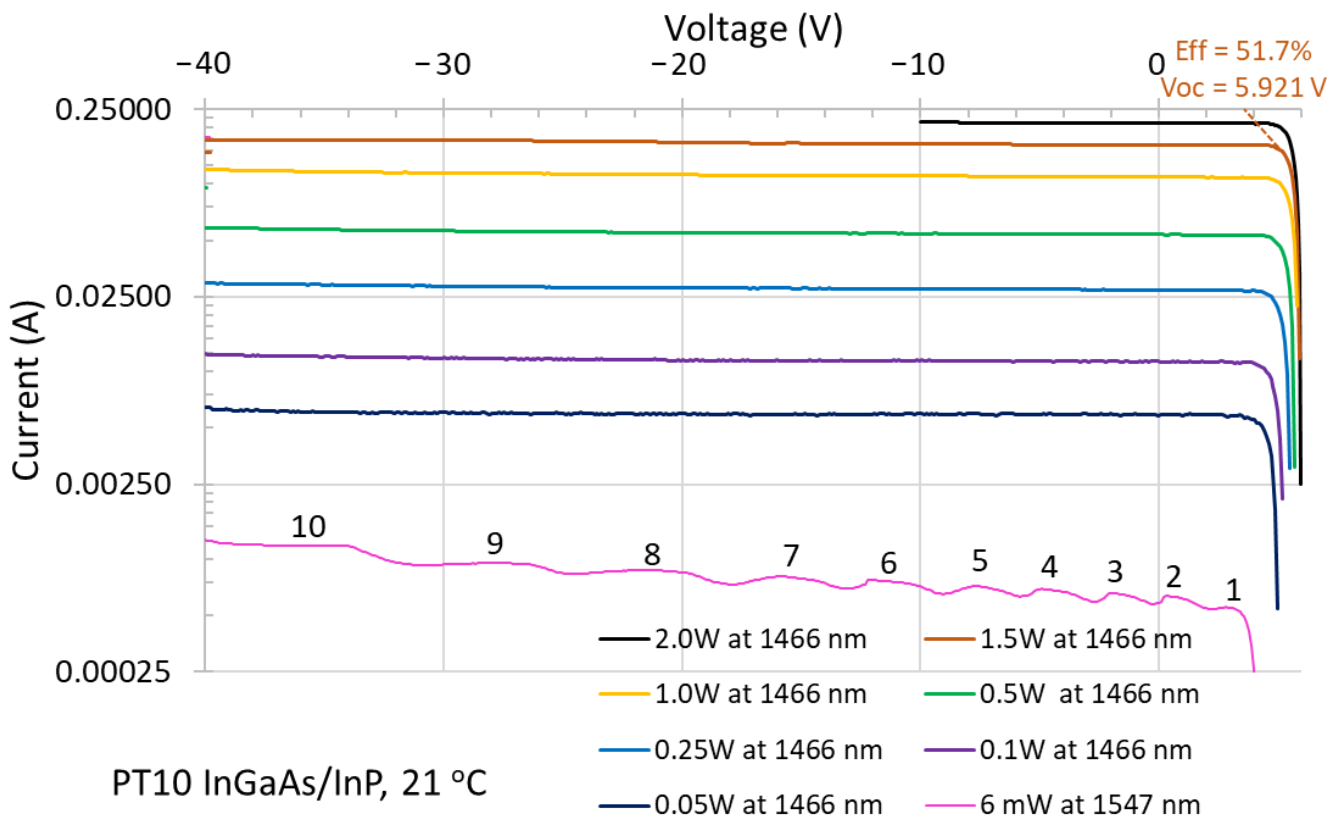


Figure 5. Measured I–V characteristics of a PT10 multijunction device with 10 InGaAs subcells lattice-matched to InP. The I–V curves are measured at the wavelengths and optical input powers indicated. The device area is 0.032 cm² and the thickness of the thinnest upper subcell is 105 nm. The 1466 nm curves are for the nearly spectral-matched condition and the pink curve is for a detuned condition at 1547 nm, on the long wavelength side of the peak of the spectral response: i.e., current-limited by the thinner top subcells.

The curves probed at 1466 nm correspond to the nearly spectral-matched situation. In these almost current-matched conditions, each subcell generates a similar fraction of

photocurrents and it cannot clearly be determined specifically which subcell is current-clamping the entire heterostructure. Relatively flat I–V characteristics are obtained, even in the reverse-bias conditions. A top conversion efficiency of 51.7% was obtained for an input of 1.5 W at 1466 nm (orange curve) [46]. Furthermore, the output power reaches 1.02 W when the input power is increased to 2 W (black curve).

Figure 5 also shows the I–V measured for a detuned condition at 1547 nm, represented by the pink curve. This is on the long wavelength side of the peak of the spectral response, therefore current-limited by the thinner top subcell at a voltage bias around the maximum power point ($V_{\text{mpp}} = 5.1$ V). Very similar to the GaAs PT10 or PT12, here also for the InGaAs/InP PT10, significant negative differential photocurrent behavior can be observed for the first few plateaus. The photocurrent slightly decreases as the reverse bias voltage is increased, until the corresponding current-clamping subcell reaches its reverse breakdown condition.

The 1547 nm laser had a maximum of 6 mW of optical output because it is a single-mode laser diode with limited output capabilities. However, other measurements (not shown) carried out at higher optical powers with a multimode ~1550 nm laser diode revealed similar behaviors, comparable to the results shown in Figure 5 at 1547 nm (pink curve).

5. Conclusions

We have studied photovoltaic multijunction power-converting heterostructures with thin subcells. In this study, comparable results have been obtained covering different material systems in the near-infrared: using GaAs absorbers (spectral range between 800 nm and 850 nm), and similarly using InGaAs absorbers (spectral range between 1450 nm and 1550 nm). The observed effects are therefore clearly not specific to a given material system. The influence of the thickness of the thin absorbing subcells has also been systematically investigated by probing multijunction devices with different numbers of thin subcells. Probe wavelengths below the peak of the spectral response, near the peak of the spectral response, and above the peak of the spectral response have been investigated. It allows to unambiguously obtaining conditions with current-limited bottom subcells, near current-matched, and current-limited top subcells respectively.

Near the peak of the spectral response of the heterostructure, top conversion efficiencies were obtained. They are capable of converting high-power laser beams into electrical power with conversion efficiencies reaching greater than 60% and 50%, for the GaAs and the InP material systems, respectively. Relatively flat I–V characteristics are then obtained, even for the large reverse-bias conditions.

For optical inputs at wavelengths shorter than the peak of the spectral response, plateaus are observed in the I–V curves, as expected for subcells exhibiting reverse-bias breakdown behaviors. The reverse voltage breakdown characteristics of GaAs control of single junction subcells were separately confirmed to depend on the thickness of the subcell and on the incident optical intensity. The thinner subcells exhibit higher levels of reverse bias currents.

In contrast, for optical inputs at wavelengths longer than the peak of the spectral response, the plateaus in the I–V curves can be slightly distorted. The effect was observed to be more pronounced when the thinnest (upper) subcells have thicknesses of ~100 nm or smaller (i.e., PTN devices with larger N). Our results suggest that the application of electric fields on thin heterostructures can result in such distinctive I–V characteristics due to modifications of the absorption characteristics from Franz–Keldysh perturbations or the onset of quantum-confined Stark effects. For the thin subcells, negative differential photocurrent effects were observed until the corresponding current-clamping subcell reached its reverse breakdown condition.

For such thin subcells, the n-type emitter and the p-type base are typically designed to be individually about half of the thickness of the subcell. The built-in field of the n/p junction therefore divides the absorber into three regions. The high-field region

in the middle of the subcell, and on either side, regions forming electrons and holes with confinement potentials under the reverse bias conditions. The electron confinement potential is formed in the conduction band, nearest to the input side of the incident beam, between the built-in field and the conduction band discontinuity of the n-type cladding material. The hole confinement potential is formed in the valence band, opposite to the input side of the incident beam, between the built-in field and the valence band discontinuity of the p-type cladding material.

Characteristically, during the onset of the quantum confined Stark effect, the absorption edge of the absorber is red-shifted while typically the absorption coefficient decreases for energies above the shifted band-edge. The observed negative differential photocurrent effects are therefore consistent with such an onset of the quantum confined Stark effect.

Importantly, it should be noted that the negative differential photocurrent effects observed and described in this study do not significantly affect the maximum power point of multijunction optical power converters.

Author Contributions: Conceptualization, S.F. and D.M.; methodology, S.F. and D.M.; software, S.F. and D.M.; validation, S.F. and D.M.; formal analysis, S.F. and D.M.; investigation, S.F. and D.M.; data curation, S.F. and D.M.; writing—original draft preparation S.F.; writing—review and editing S.F. and D.M.; visualization, S.F.; project administration, S.F. and D.M.; funding acquisition, S.F. and D.M. All authors have read and agreed to the published version of the manuscript.

Funding: This research received no external funding.

Institutional Review Board Statement: Not applicable.

Informed Consent Statement: Not applicable.

Data Availability Statement: The data that support the findings of this study are available from the corresponding author upon reasonable request.

Conflicts of Interest: The authors declare no conflict of interest, but it should be noted that the authors are employed by Broadcom, a company that manufactures and sells semiconductor components, including power converter devices.

References

1. Burgiel, J.C. Electric-field-induced infrared absorption in GaAs p-n junctions. *Appl. Phys. Lett.* **1966**, *9*, 389–390. [[CrossRef](#)]
2. Miller, D.A.B.; Chemla, D.S.; Damen, T.C.; Gossard, A.C.; Wiegmann, W.; Wood, T.H.; Burrus, C.A. Band-Edge Electroabsorption in Quantum Well Structures: The Quantum-Confined Stark Effect. *Phys. Rev. Lett.* **1984**, *53*, 2173–2176. [[CrossRef](#)]
3. Miller, D.A.B.; Chemla, D.S.; Damen, T.C.; Gossard, A.C.; Wiegmann, W.; Wood, T.H.; Burrus, C.A. Electric field dependence of optical absorption near the band gap of quantum-well structures. *Phys. Rev. B* **1985**, *32*, 1043–1060. [[CrossRef](#)] [[PubMed](#)]
4. Miller, D.A.B.; Chemla, D.S.; Schmitt-Rink, S. Relation between electroabsorption in bulk semiconductors and in quantum wells: The quantum-confined Franz-Keldysh effect. *Phys. Rev. B* **1986**, *33*, 6976–6982. [[CrossRef](#)] [[PubMed](#)]
5. Jelley, K.W.; Alavi, K.; Engelmann, R.W.H. Experimental determination of electroabsorption in GaAs/Al_{0.32}Ga_{0.68}As multiple quantum well structures as function of well width. *Electron. Lett.* **1988**, *24*, 1555–1557. [[CrossRef](#)]
6. Fafard, S. Energy levels in quantum wells with capping barrier layer of finite size: Bound states and oscillatory behavior of the continuum states. *Phys. Rev. B* **1992**, *46*, 4659–4666. [[CrossRef](#)] [[PubMed](#)]
7. Fafard, S.; Fortin, E.; Merz, J.L. Excitation-intensity-dependent photoluminescence quenching due to electric-field screening by photocarriers captured in single-quantum-well structures. *Phys. Rev. B* **1993**, *48*, 11062–11066. [[CrossRef](#)]
8. Chtanov, A.; Baars, T.; Gal, M. Excitation-intensity-dependent photoluminescence in semiconductor quantum wells due to internal electric fields. *Phys. Rev. B* **1996**, *53*, 4704–4707. [[CrossRef](#)]
9. Wahlstrand, J.K.; Sipe, J.E. Independent-particle theory of the Franz-Keldysh effect including interband coupling: Application to calculation of electroabsorption in GaAs. *Phys. Rev. B* **2010**, *82*, 075206. [[CrossRef](#)]
10. Duque-Gomez, F.; Sipe, J. The Franz-Keldysh effect revisited: Electroabsorption including interband coupling and excitonic effects. *J. Phys. Chem. Solids* **2015**, *76*, 138–152. [[CrossRef](#)]
11. van Eerden, M.; van Gastel, J.; Bauhuis, G.J.; Mulder, P.; Vlieg, E.; Schermer, J.J. Observation and implications of the Franz-Keldysh effect in ultrathin GaAs solar cells. *Prog. Photovoltaics: Res. Appl.* **2020**, *28*, 779–787. [[CrossRef](#)]
12. Fafard, S.; Masson, D.P. Perspective on photovoltaic optical power converters. *J. Appl. Phys.* **2021**, *130*, 160901. [[CrossRef](#)]
13. Helmers, H.; Lopez, E.; Höhn, O.; Lackner, D.; Schön, J.; Schauerte, M.; Schachtner, M.; Dimroth, F.; Bett, A.W. 68.9% Efficient GaAs-Based Photonic Power Conversion Enabled by Photon Recycling and Optical Resonance. *Phys. Status Solidi (RRL) Rapid Res. Lett.* **2021**, *15*, 2100113. [[CrossRef](#)]

14. Algora, C.; García, I.; Delgado, M.; Peña, R.; Vázquez, C.; Hinojosa, M.; Rey-Stolle, I. Beaming power: Photovoltaic laser power converters for power-by-light. *Joule* **2022**, *6*, 340–368. [[CrossRef](#)]
15. Mukherjee, J.; Jarvis, S.; Perren, M.; Sweeney, S.J. Efficiency limits of laser power converters for optical power transfer applications. *J. Phys. D Appl. Phys.* **2013**, *46*. [[CrossRef](#)]
16. Putra, E.P.; Theivindran, R.; Hasnul, H.; Lee, H.J.; Ker, P.J.; Jamaludin, Z.; Awang, R.; Yusof, F.A.M. Technology update on patent and development trend of power over fiber: A critical review and future prospects. *J. Photon Energy* **2023**, *13*, 011001. [[CrossRef](#)]
17. Yamaguchi, M.; Dimroth, F.; Geisz, J.F.; Ekins-Daukes, N.J. Multi-junction solar cells paving the way for super high-efficiency. *J. Appl. Phys.* **2021**, *129*, 240901. [[CrossRef](#)]
18. Wang, A.-C.; Yin, J.-J.; Yu, S.-Z.; Sun, Y.-R.; Dong, J.-R. Origins of the short circuit current of a current mismatched multijunction photovoltaic cell considering subcell reverse breakdown. *Opt. Express* **2023**, *31*, 14482–14494. [[CrossRef](#)] [[PubMed](#)]
19. Fernández, E.F.; García-Loureiro, A.; Seoane, N.; Almonacid, F. Band-gap material selection for remote high-power laser transmission. *Sol. Energy Mater. Sol. Cells* **2022**, *235*, 111483. [[CrossRef](#)]
20. Beattie, M.N.; Valdivia, C.E.; Wilkins, M.M.; Zamiri, M.; Kaller, K.L.C.; Tam, M.C.; Kim, H.S.; Krich, J.J.; Wasilewski, Z.R.; Hinzner, K. High current density tunnel diodes for multi-junction photovoltaic devices on InP substrates. *Appl. Phys. Lett.* **2021**, *118*, 062101. [[CrossRef](#)]
21. Ičić, S.; Tomić, S. Genetic algorithm designed high efficiency laser power converters based on the vertical epitaxial heterostructure architecture. *Sol. Energy Mater. Sol. Cells* **2019**, *200*, 109878.
22. Masson, D.; Proulx, F.; Fafard, S. Pushing the limits of concentrated photovoltaic solar cell tunnel junctions in novel high-efficiency GaAs phototransducers based on a vertical epitaxial heterostructure architecture. *Prog. Photovolt. Res. Appl.* **2015**, *23*, 1687–1696. [[CrossRef](#)]
23. Fafard, S.; Masson, D.P. Transducer to Convert Optical Energy to Electrical Energy. U.S. Patent 9,673,343, 6 June 2017.
24. Bett, A.W.; Dimroth, F.; Lockenhoff, R.; Oliva, E.; Schubert, J. III–V solar cells under monochromatic illumination. In Proceedings of the Conference Record of the IEEE Photovoltaic Specialists Conference, San Diego, CA, USA, 11–16 May 2008; p. 4922910.
25. Oliva, E.; Dimroth, F.; Bett, A.W. GaAs converters for high power densities of laser illumination. *Prog. Photovolt. Res. Appl.* **2008**, *16*, 289–295. [[CrossRef](#)]
26. Schubert, J.; Oliva, E.; Dimroth, F.; Guter, W.; Loekenhoff, R.; Bett, A.W. High-Voltage GaAs Photovoltaic Laser Power Converters. *IEEE Trans. Electron Devices* **2009**, *56*, 170–175. [[CrossRef](#)]
27. Höhn, O.; Walker, A.W.; Bett, A.W.; Helmers, H. Optimal laser wavelength for efficient laser power converter operation over temperature. *Appl. Phys. Lett.* **2016**, *108*, 241104. [[CrossRef](#)]
28. Kimovec, R.; Helmers, H.; Bett, A.W.; Topic, M. On the Influence of the Photo-Induced Leakage Current in Monolithically Interconnected Modules. *IEEE J. Photovolt.* **2018**, *8*, 541–546. [[CrossRef](#)]
29. Kimovec, R.; Helmers, H.; Bett, A.W.; Topič, M. Comprehensive electrical loss analysis of monolithic interconnected multi-segment laser power converters. *Prog. Photovolt. Res. Appl.* **2019**, *27*, 199–209. [[CrossRef](#)]
30. Helmers, H.; Franke, A.; Lackner, D.; Hohn, O.; Predan, F.; Dimroth, F. 51% Efficient Photonic Power Converters for O-Band Wavelengths around 1310 nm. In Proceedings of the 2020 IEEE 47th Photovoltaic Specialists Conference (PVSC), virtual meeting, 15 June–21 August 2020; pp. 2471–2474.
31. Wagner, L.; Reichmuth, S.K.; Philipps, S.P.; Oliva, E.; Bett, A.W.; Helmers, H. Integrated series/parallel connection for photovoltaic laser power converters with optimized current matching. *Prog. Photovolt. Res. Appl.* **2020**, *29*, 172. [[CrossRef](#)]
32. Beattie, M.N.; Helmers, H.; Forcade, G.P.; Valdivia, C.E.; Höhn, O.; Hinzner, K. InP-and GaAs-Based Photonic Power Converters Under O-Band Laser Illumination: Performance Analysis and Comparison. *IEEE J. Photovolt.* **2022**, *13*, 113–121. [[CrossRef](#)]
33. Zhao, Y.; Sun, Y.; He, Y.; Yu, S.; Dong, J. Design and fabrication of six-volt vertically-stacked GaAs photovoltaic power converter. *Sci. Rep.* **2016**, *6*, 38044. [[CrossRef](#)]
34. Ding, Y.; Li, Q.; Lu, Y.; Wang, J. TO-packaged, multi-junction GaAs laser power converter with output electric power over 1W. In Proceedings of the 2017 Conference on Lasers and Electro-Optics Pacific Rim (CLEO-PR), Singapore, 31 July–4 August 2017; pp. 1–3.
35. Sun, Y.-R.; Dong, J.-R.; He, Y.; Zhao, Y.-M.; Yu, S.-Z.; Xue, J.-P.; Xue, C.; Wang, J.; Lu, Y.-Q.; Ding, Y.-W. A six-junction GaAs laser power converter with different sizes of active aperture. *Optoelectron. Lett.* **2017**, *13*, 21–24. [[CrossRef](#)]
36. Huang, J.; Sun, Y.; Zhao, Y.; Yu, S.; Li, K.; Dong, J.; Xue, J.; Xue, C.; Ye, Y. Characterizations of high-voltage vertically-stacked GaAs laser power converter. *J. Semicond.* **2018**, *39*, 094006. [[CrossRef](#)]
37. Huang, J.; Sun, Y.; Zhao, Y.; Yu, S.; Dong, J.; Xue, J.; Xue, C.; Wang, J.; Lu, Y.; Ding, Y. Four-junction AlGaAs/GaAs laser power converter. *J. Semicond.* **2018**, *39*, 044003. [[CrossRef](#)]
38. Yin, J.; Sun, Y.; Yu, S.; Zhao, Y.; Li, R.; Dong, J. 1064 nm InGaAsP multi-junction laser power converters. *J. Semicond.* **2020**, *41*, 062303. [[CrossRef](#)]
39. Wang, A.-C.; Sun, Y.-R.; Yu, S.-Z.; Yin, J.-J.; Zhang, W.; Wang, J.-S.; Fu, Q.-X.; Dong, J.-R. A method to analyze current mismatch in a multijunction laser power converter based on I–V measurements. *Appl. Phys. Lett.* **2021**, *118*, 233902. [[CrossRef](#)]
40. Wang, A.-C.; Sun, Y.-R.; Yu, S.-Z.; Yin, J.-J.; Zhang, W.; Wang, J.-S.; Fu, Q.-X.; Han, Y.-H.; Qin, J.; Dong, J.-R. Characteristics of 1520 nm InGaAs multijunction laser power converters. *Appl. Phys. Lett.* **2021**, *119*, 243902. [[CrossRef](#)]
41. Wang, A.-C.; Yin, J.-J.; Yu, S.-Z.; Sun, Y.-R. Multiple tunnel diode peaks in I–V curves of a multijunction laser power converter. *Appl. Phys. Lett.* **2022**, *121*, 233901. [[CrossRef](#)]

42. Fafard, S.; York, M.C.A.; Proulx, F.; Valdivia, C.E.; Wilkins, M.M.; Arès, R.; Aimez, V.; Hinzer, K.; Masson, D.P. Ultrahigh efficiencies in vertical epitaxial heterostructure architectures. *Appl. Phys. Lett.* **2016**, *108*, 071101. [[CrossRef](#)]
43. Fafard, S.; Proulx, F.; York, M.C.A.; Richard, L.S.; Provost, P.O.; Arès, R.; Aimez, V.; Masson, D.P. High-photovoltage GaAs vertical epitaxial monolithic heterostructures with 20 thin p/n junctions and a conversion efficiency of 60%. *Appl. Phys. Lett.* **2016**, *109*, 131107. [[CrossRef](#)]
44. York, M.C.; Fafard, S. High efficiency phototransducers based on a novel vertical epitaxial heterostructure architecture (VEHSA) with thin p/n junctions. *J. Phys. D Appl. Phys.* **2017**, *50*, 173003. [[CrossRef](#)]
45. Fafard, S.; Masson, D.; Werthen, J.-G.; Liu, J.; Wu, T.-C.; Hundsberger, C.; Schwarzfischer, M.; Steinle, G.; Gaertner, C.; Piemonte, C.; et al. Power and Spectral Range Characteristics for Optical Power Converters. *Energies* **2021**, *14*, 4395. [[CrossRef](#)]
46. Fafard, S.; Masson, D.P. High-Efficiency and High-Power Multijunction InGaAs/InP Photovoltaic Laser Power Converters for 1470 nm. *Photonics* **2022**, *9*, 438. [[CrossRef](#)]
47. Fafard, S.; Masson, D.P. 74.7% Efficient GaAs-based laser power converters at 808 nm at 150 K. *Photonics* **2022**, *9*, 579. [[CrossRef](#)]
48. Fafard, S.; Masson, D.P. Vertical Multi-Junction Laser Power Converters with 61% Efficiency at 30 W Output Power and with Tolerance to Beam Non-Uniformity, Partial Illumination, and Beam Displacement. *Photonics* **2023**, *10*, 940. [[CrossRef](#)]
49. Andreev, V.; Khvostikov, V.; Kalinovsky, V.; Lantratov, V.; Grilikhes, V.; Rummyantsev, V.; Shvarts, M.; Fokanov, V.; Pavlov, A. High current density GaAs and GaSb photovoltaic cells for laser power beaming. In Proceedings of the 3rd World Conference on Photovoltaic Energy Conversion, Osaka, Japan, 11–18 May 2003; Volume 1, pp. 761–764.
50. Khvostikov, V.P.; Kalyuzhnyy, N.A.; Mintairov, S.A.; Sorokina, S.V.; Potapovich, N.S.; Emelyanov, V.M.; Timoshina, N.K.; Andreev, V.M. Photovoltaic laser-power converter based on AlGaAs/GaAs heterostructures. *Semiconductors* **2016**, *50*, 1220–1224. [[CrossRef](#)]
51. Khvostikov, V.P.; Sorokina, S.V.E.; Potapovich, N.S.; Khvostikova, O.G.A.E.; Timoshina, N.K. Laser ($\lambda = 809$ nm) power converter based on GaAs. *Semiconductors* **2017**, *51*, 645–648. [[CrossRef](#)]
52. Khvostikov, V.P.; Sorokina, S.V.; Potapovich, N.S.; Khvostikova, O.A.; Timoshina, N.K.; Shvarts, M.Z. Modification of Photovoltaic Laser-Power ($\lambda = 808$ nm) Converters Grown by LPE. *Semiconductors* **2018**, *52*, 366–370. [[CrossRef](#)]
53. Khvostikov, V.P.; Sorokina, S.V.; Khvostikova, O.A.; Potapovich, N.S.; Malevskaya, A.V.; Nakhimovich, M.V.; Shvarts, M.Z. GaSb photovoltaic cells for laser power conversion. In Proceedings of the 15th International Conference on Concentrator Photovoltaic Systems (CPV-15), Fes, Morocco, 25–27 March 2019; p. 050007.
54. Panchak, A.; Khvostikov, V.; Pokrovskiy, P. AlGaAs gradient waveguides for vertical p/n junction GaAs laser power converters. *Opt. Laser Technol.* **2021**, *136*, 106735. [[CrossRef](#)]
55. Khvostikov, V.P.; Panchak, A.N.; Khvostikova, O.A.; Pokrovskiy, P.V. Side-input GaAs laser power converters WITH gradient AlGaAs waveguide. *IEEE Electron Device Lett.* **2022**, *43*, 1717–1719. [[CrossRef](#)]
56. Khvostikov, V.P.; Sorokina, S.V.; Khvostikova, O.A.; Nakhimovich, M.V.; Shvarts, Z. Ge-Based Photovoltaic Laser-Power Converters. *IEEE J. Photovolt.* **2023**, *13*, 254–259. [[CrossRef](#)]
57. Proulx, F.; York, M.C.A.; Provost, P.O.; Arès, R.; Aimez, V.; Masson, D.P.; Fafard, S. Measurement of strong photon recycling in ultra-thin GaAs n/p junctions monolithically integrated in high-photovoltage vertical epitaxial heterostructure architectures with conversion efficiencies exceeding 60%. *Phys. Status Solidi (RRL) Rapid Res. Lett.* **2016**, *11*, 1600385. [[CrossRef](#)]
58. Wilkins, M.; Valdivia, C.E.; Gabr, A.M.; Masson, D.; Fafard, S.; Hinzer, K. Luminescent coupling in planar opto-electronic devices. *J. Appl. Phys.* **2015**, *118*, 143102. [[CrossRef](#)]
59. Lopez, E.; Höhn, O.; Schauerte, M.; Lackner, D.; Schachtner, M.; Reichmuth, S.K.; Helmers, H. Experimental coupling process efficiency and benefits of back surface reflectors in photovoltaic multi-junction photonic power converters. *Prog. Photovolt. Res. Appl.* **2021**, *29*, 461–470. [[CrossRef](#)]
60. Xia, D.; Krich, J.J. Efficiency increase in multijunction monochromatic photovoltaic devices due to luminescent coupling. *J. Appl. Phys.* **2020**, *128*, 013101. [[CrossRef](#)]
61. Law, H.D.; Ng, W.W.; Nakano, K.; Dapkus, P.D.; Stone, D.R. High Efficiency InGaAsP Photovoltaic Power Converter. *IEEE Electron Device Lett.* **1981**, *2*, 26–27. [[CrossRef](#)]
62. Olsen, L.C.; Huber, D.A.; Dunham, G.; Addis, F.W. High efficiency monochromatic GaAs solar cells. In Proceedings of the Conference Record of the IEEE Photovoltaic Specialists Conference, Las Vegas, NV, USA, 7–11 October 1991; pp. 419–424.
63. Green, M.; Zhao, J.; Wang, A.; Wenham, S. 45% Efficient Silicon Photovoltaic Cell under Monochromatic Light. *IEEE Electron Device Lett.* **1992**, *13*, 317–318. [[CrossRef](#)]
64. Fahrenbruch, A.L.; Lopez-Otero, L.; Werthern, J.G.; Wu, T.C. GaAs- and InAlGaAs-based concentrator-type cells for conversion of power transmitted by optical fibers. In Proceedings of the Conference Record of the IEEE Photovoltaic Specialists Conference, Washington, DC, USA, 13–17 May 1996; pp. 117–120.
65. Fave, A.; Kaminski, A.; Gavand, M.; Mayet, L.; Laugier, A. GaAs converter for high power laser diode. In Proceedings of the Conference Record of the IEEE Photovoltaic Specialists Conference, Washington, DC, USA, 13–17 May 1996; pp. 101–104.
66. Wojtczuk, S.J. Long-wavelength laser power converters for optical fibers. In Proceedings of the Conference Record of the Twenty Sixth IEEE Photovoltaic Specialists Conference, Anaheim, CA, USA, 29 September–3 October 1997; pp. 971–974.
67. Peña, R.; Algora, C.; Anton, I. GaAs multiple photovoltaic converters with an efficiency of 45% for monochromatic illumination. In Proceedings of the 3rd World Conference on Photovoltaic Energy Conversion, Osaka, Japan, 11–18 May 2003; pp. 228–231.

68. Krut, D.; Sudharsanan, R.; Isshiki, T.; King, R.; Karam, N. A 53% high efficiency GaAs vertically integrated multi-junction laser power converter. In Proceedings of the 2007 65th Annual Device Research Conference, South Bend, IN, USA, 18–20 June 2007; pp. 123–124.
69. Eggert, N.; Rusack, R.; Mans, J. Evaluation of photonic power converters. *J. Instrum.* **2010**, *5*, T02001. [[CrossRef](#)]
70. Jarvis, S.D.; Mukherjee, J.; Perren, M.; Sweeney, S.J. Development and characterisation of laser power converters for optical power transfer applications. *IET Optoelectron.* **2014**, *8*, 64–70. [[CrossRef](#)]
71. Shan, T.; Qi, X. Design and optimization of GaAs photovoltaic converter for laser power beaming. *Infrared Phys. Technol.* **2015**, *71*, 144–150. [[CrossRef](#)]
72. Jomen, R.; Tanaka, F.; Akiba, T.; Ikeda, M.; Kiryu, K.; Matsushita, M.; Maenaka, H.; Dai, P.; Lu, S.; Uchida, S. Conversion efficiencies of single-junction III–V solar cells based on InGaP, GaAs, InGaAsP, and InGaAs for laser wireless power transmission. *Jpn. J. Appl. Phys.* **2018**, *57*, 08RD12. [[CrossRef](#)]
73. Kalyuzhnyy, N.A.; Emelyanov, V.M.; Mintairov, S.A.; Shvarts, M.Z. InGaAs metamorphic laser ($\lambda=1064$ nm) power converters with over 44% efficiency. In Proceedings of the 14th International Conference on Concentrator Photovoltaic Systems (CPV-14), Puertollano, Spain, 16–18 April 2018; p. 110002.
74. Ičić, S.; Tomić, S. Automated design of multi junction solar cells by genetic approach: Reaching the >50% efficiency target. *Sol. Energy Mater. Sol. Cells* **2018**, *181*, 30–37.
75. Kim, Y.; Shin, H.-B.; Lee, W.-H.; Jung, S.H.; Kim, C.Z.; Kim, H.; Lee, Y.T.; Kang, H.K. 1080 nm InGaAs laser power converters grown by MOCVD using InAlGaAs metamorphic buffer layers. *Sol. Energy Mater. Sol. Cells* **2019**, *200*, 109984. [[CrossRef](#)]
76. Panchak, A.N.; Pokrovskiy, P.V.; Malevskiy, D.A.; Larionov, V.R.; Shvarts, M.Z. High-Efficiency Conversion of High-Power-Density Laser Radiation. *Tech. Phys. Lett.* **2019**, *45*, 24–26. [[CrossRef](#)]
77. Zhao, Y.; Liang, P.; Ren, H.; Han, P. Enhanced efficiency in 808 nm GaAs laser power converters via gradient doping. *AIP Adv.* **2019**, *9*, 105206. [[CrossRef](#)]
78. Keller, G. GaAs multi-junction laser power converters at AZUR SPACE: Current status and development activities. In Proceedings of the 1st Optical Wireless and Fiber Power Transmission Conference (OWPT2019), Yokohama, Japan, 23 April 2019–25 April 2019; pp. 11–12.
79. Kalyuzhnyy, N.A.; Emelyanov, V.M.; Evstropov, V.V.; Mintairov, S.A.; Mintairov, M.A.; Nahimovich, M.V.; Saliu, R.A.; Shvarts, M.Z. Optimization of photoelectric parameters of InGaAs metamorphic laser ($\lambda = 1064$ nm) power converters with over 50% efficiency. *Sol. Energy Mater. Sol. Cells* **2020**, *217*, 110710. [[CrossRef](#)]
80. Komuro, Y.; Honda, S.; Kurooka, K.; Warigaya, R.; Tanaka, F.; Uchida, S. A 43.0% efficient GaInP photonic power converter with a distributed Bragg reflector under high-power 638nm laser irradiation of 17Wcm^{-2} . *Appl. Phys. Express* **2021**, *14*, 052002. [[CrossRef](#)]
81. Lin, M.; Sha, W.E.I.; Zhong, W.; Xu, D. Intrinsic losses in photovoltaic laser power converters. *Appl. Phys. Lett.* **2021**, *118*, 104103. [[CrossRef](#)]
82. Zhao, Y.; Li, S.; Ren, H.; Li, S.; Han, P. Energy band adjustment of 808 nm GaAs laser power converters via gradient doping. *J. Semicond.* **2021**, *42*, 032701. [[CrossRef](#)]
83. Nouri, N.; Valdivia, C.E.; Beattie, M.N.; Zamiri, M.S.; Krich, J.J.; Hinzer, K. Ultrathin monochromatic photonic power converters with nanostructured back mirror for light trapping of 1310-nm laser illumination. In Proceedings of the Physics, Simulation, and Photonic Engineering of Photovoltaic Devices X, San Francisco, CA, USA, 5 March 2021; p. 116810X.
84. Kurooka, K.; Honda, T.; Komazawa, Y.; Warigaya, R.; Uchida, S. A 46.7% efficient GaInP photonic power converter under high-power 638 nm laser uniform irradiation of 1.5W cm^{-2} . *Appl. Phys. Express* **2022**, *15*, 062003. [[CrossRef](#)]
85. Gou, Y.; Wang, H.; Wang, J.; Zhang, Y.; Niu, R.; Chen, X.; Wang, B.; Xiao, Y.; Zhang, Z.; Liu, W.; et al. 1064 nm InGaAs metamorphic laser power converts with over 44% efficiency. *Opt. Express* **2022**, *30*, 42178–42185. [[CrossRef](#)]
86. Yin, J.; Sun, Y.; Wang, A.; Yu, S.; Wang, J.; Fu, Q.; Qin, J.; Han, Y.; Zhang, W.; Zhang, S.; et al. High-Voltage 1064 nm InGaAsP Multijunction Laser Power Converters. *IEEE Electron Device Lett.* **2022**, *43*, 1291–1294. [[CrossRef](#)]
87. Chancerel, F.; Regreny, P.; Leclercq, J.L.; Volatier, M.; Jaouad, A.; Darnon, M.; Fafard, S.; Gendry, M.; Aimez, V. Comparison of various InGaAs-based solar cells for concentrated photovoltaics applications. In Proceedings of the AIP Conference Proceedings, Freiburg, Germany, 12–14 April 2021; p. 2550.
88. Wang, H.; Wang, J.; Yang, H.; Deng, G.; Yang, Q.; Niu, R.; Gou, Y. The Effect of Non-Uniform Irradiation on Laser Photovoltaics: Experiments and Simulations. *Photonics* **2022**, *9*, 493. [[CrossRef](#)]
89. Lozano, J.F.; Seoane, N.; Comesana, E.; Almonacid, F.; Fernández, E.F.; García-Loureiro, A. Laser Power Converter Architectures Based on 3C-SiC with Efficiencies >80%. *Sol. RRL* **2022**, *6*, 2101077. [[CrossRef](#)]
90. Martinek, P.; Prajzler, V. Power over fiber using a large core fiber and laser operating at 976 nm with 10 W power. *Opt. Fiber Technol.* **2023**, *80*, 103404. [[CrossRef](#)]
91. Geisz, J.F.; Friedman, D.J.; Steiner, M.A.; France, R.M.; Song, T. Operando Temperature Measurements of Photovoltaic Laser Power Converter Devices Under Continuous High-Intensity Illumination. *IEEE J. Photovolt.* **2023**, *13*, 808–813. [[CrossRef](#)]

Disclaimer/Publisher’s Note: The statements, opinions and data contained in all publications are solely those of the individual author(s) and contributor(s) and not of MDPI and/or the editor(s). MDPI and/or the editor(s) disclaim responsibility for any injury to people or property resulting from any ideas, methods, instructions or products referred to in the content.